Glassy Protein Dynamics and Gigantic Solvent Reorganization Energy of Plastocyanin

David N. LeBard and Dmitry V. Matyushov*

Center for Biological Physics, Arizona State University, P.O. Box 871604, Tempe, Arizona 85287-1604

Received: October 1, 2007; In Final Form: February 1, 2008

We report the results of molecular dynamics simulations of electron-transfer activation parameters of plastocyanin metalloprotein involved as an electron carrier in natural photosynthesis. We have discovered that slow, non-ergodic conformational fluctuations of the protein, coupled to hydrating water, result in a very broad distribution of donor−acceptor energy gaps far exceeding those observed for commonly studied inorganic and organic donor−acceptor complexes. The Stokes shift is not affected by these fluctuations and can be calculated from solvation models in terms of the linear response of the solvent dipolar polarization. The non-ergodic character of large-amplitude protein/water mobility breaks the strong link between the Stokes shift and the reorganization energy characteristic of equilibrium (ergodic) theories of electron transfer. This mechanism might be responsible for fast electronic transitions in natural electron-transfer proteins characterized by low reaction free energy.

I. Introduction

Redox proteins play diverse roles as electron carriers in biological energy chains.[1] Enzymatic activity often involves transferring electrons to carry chemical reactions,[2] while metalloproteins deposited in mitochondrial membranes and photosynthetic units serve as redox sites with a tuned redox potential to allow one-directional electron flow in electron-transfer chains.[3] Plastocyanin (PC) from spinach is a single polypeptide chain of 99 residues forming a β-sandwich, with a single copper ion coordinated by two sulfurs from cysteine and methionine and two nitrogens from histidine residues (Figure 1). The presence of the copper ion, which can change the redox state, allows PC to function as a mobile electron carrier in the photosynthetic apparatus of plants and bacteria. It accepts an electron from ferrocytochrome *f* and diffusionally carries it to another docking location where the electron is donated to the oxidized form of Photosystem I.[4]

This functionality is achieved through fast electron-transfer reactions at docking locations with a low driving force $\simeq$ 20 meV and an electron tunneling distance > 10 Å.[4] The efficient turnover of the photosynthetic apparatus demands fast rates at redox sites, faster than typical biological catalytic rates of 10^2−10^4 s^{-1} (ref 3). Given the small driving force, this constraint limits the reorganization energy $\lambda_s + \lambda_v$ to about 1 eV.[5] The reorganization energy here is a sum of the solvent, λ_s, and internal vibrational, λ_v, components. In the rest of this paper, we will separate the atoms with partial charges varying with the redox state as the redox site (Figure 1), considering the rest of the protein and water as the thermal bath. The internal reorganization energy λ_v then refers to vibrational nuclear modes of the active site, while, in the case of protein electron transfer, the thermal bath generally incorporates the combined electrostatic effect of the protein and water. Our main focus will, however, be on the interaction of the redox site with water, and that is how, following the established tradition,[6] we define the solvent reorganization energy λ_s separating the interactions with the protein atomic charges into the protein reorganization energy λ_{prot} (see below for a more precise definition).

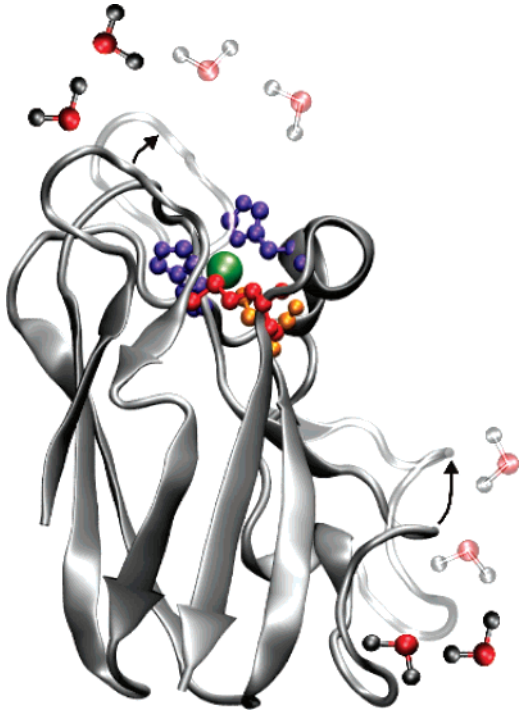

Figure 1. Structure of plastocyanin and the illustration of the protein large-scale conformational motions displacing hydrating water. The active site includes a copper ion (green), two histidines (blue), methionine (red), and cysteine (orange) residues. The arrows and transparent parts of the protein illustrate motions of the main chain loops (not from actual MD simulations) displacing water molecules.

Both λ_v and λ_s are large in synthetic redox systems with a copper ion serving as the redox site because of large structural changes upon electron transfer and a strong electrostatic interaction of copper with polar solvents. Much less is known about electron transfer in and between copper proteins. Experimental measurements[7] and quantum calculations[8] of the internal reorganization energy of copper proteins are still inconclusive,

* To whom correspondence should be addressed.

10.1021/jp709586e CCC: $40.75
Published on Web 03/15/2008 PAGE EST: 9.9

placing it between 0.1 eV[8] and 0.6−0.7 eV (ref 7 and references therein). In addition, recent numerical simulations of heme and copper proteins have uniformly placed their solvent reorganization energies in the range of 0.5−1.0 eV.[2,8−12] These calculations give results somewhat higher than what follows from the experimental work on Ru-modified *aeruginoza* azurin, which has shown that the activation barrier disappears at $\lambda_s + \lambda_v \simeq 0.6-0.8$ eV.[13]

Even if the internal reorganization energy is as low as 0.1 eV,[8] the available data suggest that electronic transitions involving copper proteins are significantly constrained thermodynamically, requiring tight docking configurations[14] and strong electronic overlaps within the donor−acceptor pair, which can be modulated by protein conformations.[15] One therefore wonders if there are possibly some mechanisms at play which are not included in standard models of electron transfer[6] but which might allow a greater tolerance in varying the parameters affecting the activation barrier. Our simulations reported here in fact show that the combination of charged surface residues with the coupled protein/water dynamics[16−18] leads to a lower activation barrier without requiring either a larger driving force or a higher electronic overlap. PC is used here as a prototype of what may apply to many other proteins, given that the protein/water fluctuations found here are likely to be encountered among other proteins not necessarily involved in redox activity.[19]

II. Energetics of Electron Transfer

Electron-transfer reactions are driven by thermal fluctuations of the nuclear degrees of freedom interacting with the electronic states of the donor and acceptor. For a typical solution electron-transfer reaction, once the intramolecular skeletal vibrations are separated out,[20] the kinetics of the reaction can be represented as a transition along the solvent reaction coordinate X representing the difference of the interaction potentials between the donor−acceptor complex and the solvent in two electronic states, $X = \Delta V_{0s}$. In this case, "0" stands for the donor−acceptor complex, the redox site in this study, and "s" stands for the solvent. The energy gap ΔE between the donor and acceptor electronic levels then defines the reaction transition state by requiring $\Delta E = 0$.[21,22] This energy gap is a sum of the gas-phase component ΔE^{gas} and X

$$\Delta E = \Delta E^{gas} + X \tag{1}$$

Electrostatic interactions between the atomic partial charges of the redox site with the partial charges or multipoles of the solvent are typically included in ΔV_{0s}, although induction and dispersion nonelectrostatic interactions can be a part of the solvent energy gap as well.[23,24] Electrostatic solute−solvent coupling usually follows the rules of the linear response approximation[11,25,26] embodied in the Marcus theory of electron transfer.[6] The activation barrier is calculated in this picture from the crossing of two parabolic free-energy surfaces $G_i(X)$ (Figure 2).

Several fundamental relations for the energetics of electron transfer follow from the two basic components of the model: the use of equilibrium statistical mechanics and the linear response approximation. The first relation is the requirement of energy conservation within Boltzmann statistics[22]

$$G_2(X) = G_1(X) + \Delta E^{gas} + X \tag{2}$$

The second, the consequence of the linear response approximation, is the connection between spectroscopically[27] observable parameters of the model, the difference in equilibrium vertical energy gaps (ΔX, Stokes shift) and the variance of the energy gap ($\sigma_s^2 = \langle(\delta X)^2\rangle$, spectral width)

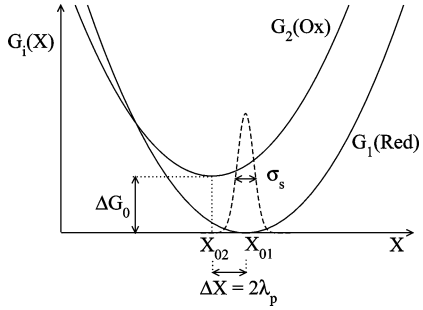

Figure 2. Two parabolas picture of electron-transfer activation.[6] The free-energy surfaces $G_i(X)$ are plotted against the solvent reaction coordinate X. The minima of the free-energy surfaces at X_{0i} ($i = 1$, Red and $i = 2$, Ox) are separated by the Stokes shift $\Delta X = X_{01} - X_{02}$, which can be used to determine the reorganization energy λ_p according to eq 4. The dashed line shows the equilibrium distribution $P_2(X) \propto \exp[-G_2(X)/(k_BT)]$ characterized by the Gaussian (spectral) width σ_s^2 used to define the reorganization energy λ_s in eq 6. The reaction free energy ΔG_0 is the vertical separation of the free-energy minima.

$$\Delta X = X_{01} - X_{02} = \sigma_s^2/k_BT \tag{3}$$

Equation 3 provides two alternative routes to define the solvent reorganization energy of electron transfer. The first definition, which we denote as λ_p, employs the vertical transition energies connecting the reorganization energy to half of the Stokes shift

$$\lambda_p = \Delta X/2 \tag{4}$$

As we show below, λ_p can be related to linear solvation of the donor−acceptor complex by the solvent polarization field considered in traditional theories of electron transfer:[6] hence, the subscript "p" stands for polarization. The reaction free energy ΔG_0 shown in Figure 2 is the vertical separation of the free-energy minima, while the mean of two equilibrium energy gaps $\Delta G_s = (X_{01} + X_{02})/2$ can be used to determine the solvent component ΔG_s of the reaction free energy such that

$$\Delta G_0 = \Delta E^{gas} + \Delta G_s \tag{5}$$

In discussing the redox thermodynamics of PC below, we will identify $i = 1$ with the reduced (Red) state and $i = 2$ with the oxidized (Ox) state (Figure 2).

An alternative definition of the reorganization energy is through the variance (spectral width)

$$\lambda_s = \sigma_s^2/(2k_BT) \tag{6}$$

As follows from eq 3

$$\lambda_s = \lambda_p \tag{7}$$

in the standard picture of crossing parabolas (Figure 2). Many attempts,[8,11,22,25,26,28−30] including those for redox proteins,[8,11,26] have been made to test eqs 2 and 3 by looking at the statistics of electrostatic solute−solvent interactions. With some deviations, commonly attributed to nonlinear solvation, they have largely given positive results, validating the picture of two crossing parabolas. In contrast, our results here report a breakdown of both relations (eqs 2 and 3) by coupled protein/water fluctuations affecting the statistics of the donor−acceptor

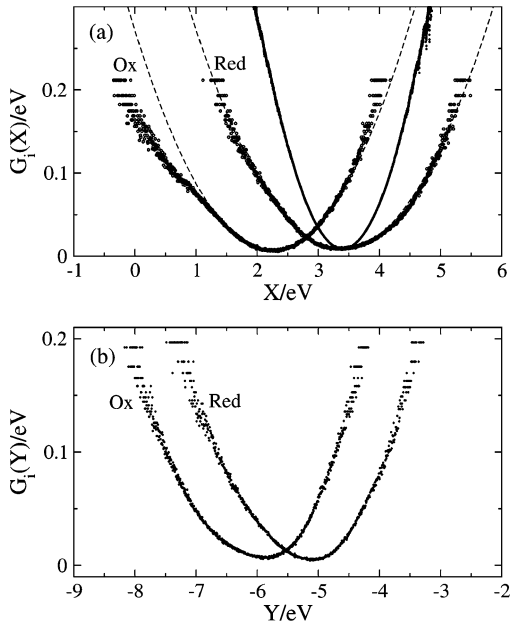

Figure 3. Electron-transfer free-energy surfaces of PC in reduced (Red) and oxidized (Ox) states at 310 K plotted against the solvent reaction coordinate X (a) and against the total (water + protein) reaction coordinate Y (b). The dashed lines in (a) are fits of $G_i(X)$ from the 10 ns trajectory to eq 11. The narrow curve in (a) has been obtained by calculating the distribution functions on 100 ps segments of the trajectory and averaging them after sliding to a common maximum. All curves are logarithms of normalized distribution functions along the corresponding reaction coordinate.

energy gap and resulting in a new component in λ_s not identified in the previous studies.

Protein electron transfer alters the standard picture of solution electron transfer by adding the protein matrix as a thermal bath interacting with the charges of the reaction site. The donor−acceptor energy gap ΔE now becomes a sum of the water component X, as in standard theories of solution electron transfer, and the electrostatic interaction with atomic charges of the protein, ΔE_{prot}. Their sum makes the total reaction coordinate

$$Y = X + \Delta E_{prot} \tag{8}$$

The variance of Y can be split into two self-correlation functions and one mixed protein/water component

$$\lambda = \langle(\delta Y)^2\rangle/(2k_BT) = \lambda_s + \lambda_{prot} + \lambda_{s,prot} \tag{9}$$

As we show below, the mixed component $\lambda_{s,prot}$ is small compared to the individual reorganization energies, which justifies the separation of the overall reorganization energy into the protein and solution parts.

The trivial extension of the standard theories of solution electron transfer to protein electron transfer given by eqs 8 and 9 encounters serious problems when applied to the analysis of our simulation data, as illustrated in Figure 3. Figure 3a shows $G_i(X)$ obtained from the calculated normalized distributions of the water component of the energy gap X, while Figure 3b shows the results obtained for the overall water/protein coordinate Y. In both cases, the reorganization energy obtained from the variance according to eq 6 exceeds by about an order of magnitude the reorganization energy obtained from the Stokes shift ΔX (eq 4) or from the overall Stokes shift ΔY. In addition, eq 2 breaks down, pointing to the non-ergodic sampling of the thermal bath statistics. Since this non-ergodic sampling of the nuclear fluctuations is relevant to electron-transfer kinetics occurring on a finite time scale,[31] we need a better grasp of the origin of this effect.

It turns out that the presence of the protein/water interface dramatically changes the statistics of water fluctuations in a way not encountered for typical small donor−acceptor complexes dissolved in dense molecular solvents. We will describe these new statistics by introducing a phenomenological model presented next, before a more detailed discussion of the simulation protocol and the results of MD simulations. The goal of this model is to introduce coupling of non-ergodic conformational protein dynamics with water fluctuations, which provides us with a general framework to understand the surprising simulation results shown in Figure 3. The main result of this model is the replacement of the solvent (water) reorganization energy λ_p of standard models[6] with the reorganization energy

$$\lambda_s = \lambda_p + \lambda_q(\tau_{obs}) \tag{10}$$

The free-energy surfaces along the solvent (water) reaction coordinate X then become

$$G_i(X) = G_{0i} + \frac{(X - X_{0i})^2}{4\lambda_s} \tag{11}$$

The new reorganization energy component $\lambda_q(\tau_{obs})$ has its predecessors in theories looking at conformational modulation of electron[32] and proton[33] transfer. However, it is the large magnitude of λ_q compared to previous estimates (reorganization energy λ_c in eq 26 from ref 32) and its non-ergodic character (dependence on the observation time τ_{obs}) that makes the problem of protein electron transfer so unique.

III. Non-ergodic Protein Conformational/Water Dynamics

Following the long-established approaches to radiationless transitions in condensed media,[21,34] we will represent the protein component of the energy gap by a linear coupling of the redox site to protein's quasi-lattice vibrations. One can then follow the standard path of introducing a spectrum of normal vibrational modes, which, for proteins, should include modes responsible for large-scale conformational mobility affecting the electrostatic potential at the redox site.[35−39] Since these likely undergo dissipative diffusional relaxation, the reaction kinetics need to be considered in a multidimensional reaction coordinate space. The physics of the classical nuclear motions in the system can be captured in terms of a two-dimensional paraboloid energy surface[40−44] as a function of classical solvent, X, and effective vibrational, q, reaction coordinates (Figure 4). The reaction coordinate in eq 8 is then a sum of X and γq, $Y = X + \gamma q$, with γ representing the electron−phonon coupling, $\Delta E_{prot} = \gamma q$. The protein component of the overall solvent reorganization energy (eq 9) is determined by the product of γ^2 and rms displacement $\langle(\delta q)^2\rangle$, $\lambda_{prot} \propto \gamma^2\langle(\delta q)^2\rangle/T$. What we however are more interested in is how to understand the profound charge in the breadth of solvent fluctuations seen in Figure 3a. We, therefore, focus in this section only on the water component of solvent reorganization.

When both modes are fully equilibrated on the reaction time scale, the reaction path $Y = X + \gamma q$ dissects the two-dimensional space along the line connecting the minima of two paraboloids. The energetic separation between the minima defines the full Stokes shift ΔY related to the overall thermal dissipation of the energy of electronic excitations by the thermal bath (Figure 4). When, on the contrary, one of the modes is slow, the reaction

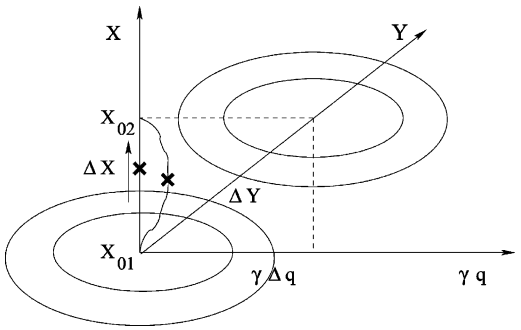

Figure 4. Electron-transfer activation in two-coordinate space including solvent coordinate X and classical conformational coordinate q (multiplied by the factor γ of electron−phonon interaction). The line connecting the two minima of the two-dimensional paraboloids corresponds to the reaction path Y for the fully thermalized fluctuations of both X and q coordinates. The total Stokes shift ΔY is then the energetic distance between the minima. Slow non-ergodic fluctuations of q shift the reaction path from the straight line connecting two equilibrium points X_{0i} to the wiggled line. The transition state then shifts from the cross point on the X-axis to a new point on the wiggled line.

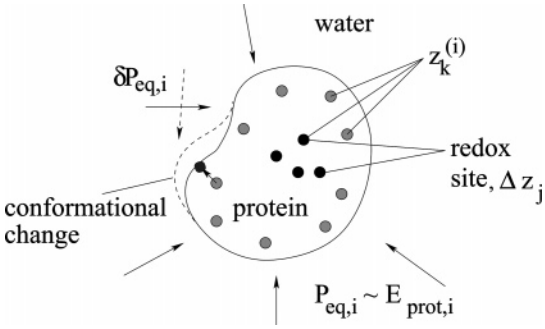

Figure 5. Schematic illustration of the alterations of the equilibrium solvent polarization by conformational motions of the protein (shown by the dashed line). The equilibrium polarization $\mathbf{P}_{eq,i}$ in the solvent (water) is proportional to the electric field of the protein $\mathbf{E}_{prot,i}$ created by its all $z_k^{(i)}$ atomic charges. Conformational changes can potentially move these charges (shown by the arrow), resulting in fluctuations of $\mathbf{E}_{prot,i}$ and the equilibrium polarization ($\delta\mathbf{P}_{eq,i}$). These fluctuations are projected onto the equilibrium energy gap $X_{0i}(q)$ in eq 13. Since the reorganization energy λ_p depends on the positions of the difference charges Δz_j of the redox site only, it is expected to be less affected by conformational fluctuations.

path deflects from the line connecting the two minima and follows the fast reaction coordinate. The final state of the reaction then falls on the X-axis (fast coordinate) and is denoted by X_{02} in Figure 4. This picture, in which the solvent is a fast mode and the solute conformational mobility is a slow coordinate, was first considered by Agmon and Hopfield.[40] The problem of two-dimensional dynamics was later formalized by Sumi and Marcus who focused, in contrast, on the opposite case of fast intramolecular vibrations.[41]

The fully equilibrated path along the coordinate Y represents the lowest potential barrier between the two equilibrium points. If conformational equilibrium is not achieved on the reaction time scale $\tau_{ET} = k_{ET}^{-1}$ (k_{ET} is the electron-transfer rate), the reaction follows the path along X with the transition state marked by the cross on the X-axis (Figure 4). However, if the reaction path deviates from the straight line due to stochastic conformational motions of the protein, it potentially can pass through a lower transition state marked by the cross on the wiggled line. The result of this is the breakdown of the link between the Stokes shift along the coordinate X, given as ΔX, and the effective curvature of the free-energy surface determined by the variance of the energy gap fluctuations $\sigma_s^2 = \langle(\delta X)^2\rangle$ (eq 3). That this picture is correct in application to our present simulations is seen from comparing Figure 3a and b. The full free-energy surfaces in Figure 3b, obtained by sampling the total interaction energy Y of the redox site with both the protein and the solvent, are uniformly shifted relative to the free energies $G_i(X)$ in Figure 3a to the negative values of Y without significant change in the Stokes shift. This observation implies no structural change to the protein matrix on the simulation time scale, thus limiting the initial and final states of the reaction trajectory to axis X in Figure 4.

The modulation of the donor−acceptor energy gap by the protein non-ergodic motions, which are unable to fully explore the conformational phase space, can be modeled by stochastic noise, in contrast to the equilibrium distribution used to derive eq 2. This effect is accounted for by adding an average over conformational fluctuations (subscript "q") to the Gaussian distribution along the solvent reaction coordinate

$$e^{-G_i(X)/k_BT} \propto \left\langle \exp\left[-\frac{(X - X_{0i}(q))^2}{4k_BT\lambda_p}\right]\right\rangle_q \qquad (12)$$

Here, the dependence on q comes to the vertical energy gap

$$X_{0i}(q) = -\mathbf{P}_{eq,i}(q) * \Delta\mathbf{E}_0 \qquad (13)$$

where the asterisk refers to both the scalar product and space integration. This gap is formed by equilibrium solvent (nuclear) polarization $\mathbf{P}_{eq,i}(q,\mathbf{r})$ in response to all partial charges $z_k^{(i)}$ of the protein (k runs over all 1439 atomic charges for PC) and the difference electric field $\Delta\mathbf{E}_0(\mathbf{r})$ created by the difference charges Δz_j of the redox site (Table S1, j runs over four atoms of the redox site for PC).

In the linear response approximation, the polarization $\mathbf{P}_{eq,i}(q,\mathbf{r})$ is linearly related to the electric field $\mathbf{E}_{prot,i}(q,\mathbf{r})$ created in the surrounding solvent by all atomic charges $z_k^{(i)}$ of the protein (Figure 5). This electric field, and therefore $\mathbf{P}_{eq,i}(q,\mathbf{r})$, is affected by the positions of these charges $r_k^{(i)}$, which can potentially be altered by conformational motions of the protein. In particular, the motions of surface-charged and polar residues, which become active above the dynamic transition temperature T_{tr},[17] can potentially modulate $\mathbf{P}_{eq,i}(q,\mathbf{r})$. On the contrary, the polarization reorganization energy λ_p is calculated as the solvation free energy of charges Δz_j of the relatively rigid redox site (Figure 5) and is affected by positions of only a few atoms (four in our simulations; see section IV). Therefore, one can expect that it is the vertical gap that is predominantly modulated by protein motions (hence the dependence of $X_{0i}(q)$ on q in eqs 12 and 13), while λ_p is mostly insensitive to such fluctuations (see below).

Assuming Gaussian statistics of δq and a linear expansion of $X_{0i}(q)$ in eq 13 in δq ($X_{0i}(q) \simeq X_{0i} + F\delta q$), one gets eqs 10 and 11. The new reorganization energy $\lambda_q(\tau_{obs})$, in principle, carries the dependence on the redox state ($i = 1,2$), which requires nonparabolic free-energy surfaces[31] and is not considered here; eq 11 in fact fits our simulation results reasonably well (the dashed lines in Figure 3a).

The reorganization energy $\lambda_q(\tau_{obs})$ carries the dependence on the observation time τ_{obs} in order to stress its non-ergodic character,[31,43] contrasting with equilibrium averages referring to $\tau_{obs} \to \infty$. The necessity to consider non-ergodic activation parameters arises from a wide spectrum of relaxation times, typical of proteins, which includes α-relaxation and a hierarchy of β-relaxations (see below). The $\lambda_q(\tau_{obs})$ arises from the protein motions fast enough to produce energy gap fluctuations in the

time frame τ_{obs} used to collect the averages, while the slower modes become dynamically arrested and do not contribute to the fluctuations of the energy gap. In view of this restriction on active modes, the reorganization energy can be obtained as the frequency integral of the autocorrelation function $C_q(\omega) = \langle|\delta q_\omega|^2\rangle$ of δq_ω, with the low-frequency cutoff reflecting the final observation time[31]

$$\lambda_q(\tau_{obs}) = (F^2/k_BT)\int_{\tau_{obs}^{-1}}^{\infty} C_q(\omega)d\omega \quad (14)$$

It turns into equilibrium reorganization energy

$$\lambda_q = F^2/(2\kappa) \quad (15)$$

(κ is an effective force constant of harmonic conformational motions) in the limit $\tau_{obs} \rightarrow \infty$ considered by statistical mechanics. The parameter F here is the slope of the donor−acceptor energy gap versus the harmonic deviation δq of the conformational mode q from equilibrium. A similar parameter appeared in previous models of conformationally affected electron[32] and proton[33] transfer.

The conformationally induced variance of the donor−acceptor energy gap

$$\sigma_q^2(T_{kin}) = 2k_BT_{kin}\lambda_q(T_{kin}) \quad (16)$$

is, in principle, accessible experimentally from heterogeneous electron-transfer kinetics measured on proteins cryogenically quenched in their conformational substates.[37] Here, the temperature of kinetic arrest T_{kin} is estimated by requiring that the quenching rate $Q = dT/dt$ and the temperature derivative of the conformational relaxation time τ_q produce unity in their product, $Q \times (d\tau_q/dT) = 1$.[45] This approach, however, eliminates the hydration dynamics facilitating conformational changes (see below). One can therefore expect that such experiments will inevitably underestimate σ_q^2 observed at high temperatures.

The phenomenological arguments presented in this section are not meant to give an accurate theoretical description of the complex non-ergodic kinetics of electron transfer influenced by protein/water dynamics. They are more intended to set up a framework to understand the results of MD simulations which provide a more detailed picture of the nuclear modes involved in the modulation of the donor−acceptor energy gap.

IV. Computational Methods

A. MD Simulations. Amber 8.0[46] was used for all MD simulations. The initial configuration of PC was created using the X-ray crystal structure at 1.7 Å resolution (PDB: 1ag6[47]). The system was heated in a NVT ensemble for 30 ps from 0 K to the desired temperature followed by volume expansion in a 1 ns NPT run. After density equilibration, NVT production runs lasting from 15 (at 310 K) to 18 ns (at 285 K) were made, of which 10 ns at the end of each trajectory were used to calculate the averages. The length of the simulations was determined by monitoring the convergence of the solvent reorganization energy λ_s, which is the slowest-converging energetic parameter calculated here. The simulation of two redox states at 285 and 310 K required 1.17−1.33 CPU years followed by 200−220 CPU days for the analysis. The computational load of parallel simulations was split between HP Alpha EV7 and Xeon/3.2GHz processors at Pittsburgh and Arizona supercomputer centers, respectively.

The time step for all MD simulations was 2 fs, and SHAKE was employed to constrain bonds to hydrogen atoms. Constant pressure and temperature simulations employed a Berendsen barostat and thermostat, respectively.[48] The long-range electrostatic interactions were handled using a smooth particle mesh Ewald summation with a 9 Å limit in the direct space sum. The total charge for the protein was −9.0 for the Red state and −8.0 for the Ox state. Each state was neutralized with the corresponding number of sodium ions, and the TIP3P model was used for water.[49]

Three atomic charging schemes were utilized to parametrize PC's redox site (Table S1). For the first parameter set, a chemically fake charging scheme was employed that uses a typical Amber force field (FF03[50]) for all standard amino acid residues but assigns an integer charge to the copper center in the reduced and oxidized states (Q1). Second, a more accurate charging scheme was based upon experimental spin densities from Solomon's group for the copper and copper ligands.[7,51] Finally, a third charge distribution was completely parametrized at the DFT level for the charges and force constants of the copper and ligand atoms and consistent with the Amber force field (Q3).[52] In addition, Amber FF03 parametrization[50] was applied to all nonligand residues (Q2). There were various numbers of TIP3P water molecules for each of the charge distributions: 5,874 (Q1), 5,886 (Q2), and 4,628 (Q3) for the Ox state and 5,873 (Q1), 5,885 (Q2), and 4,627 (Q3) for the Red state. The lower number of water molecules in the Q3 simulations was used to test the sensitivity of the results to the size of the simulation box.

We ran separate simulations (ca. 5 ns) for each charging scheme to find that the results are not strongly affected by the choice of atomic charges and/or number of water molecules. This low sensitivity to the charging scheme of the reaction site was also noticed in some other recent simulations.[8,11] We have therefore implemented charge scheme Q2 in all simulations reported here since it presents a good balance between being simple and realistic. All of the production runs reported here were done with 5886 (Ox) and 5885 (Red) water molecules.

The Amber force field[50] was also used for the ground-state tryptophan. Charges in the ^1L_a excited state were taken from the literature.[53] This charge set was chosen because it gives a good agreement with ab initio calculations of the indole ring.[54] NVT simulations of tryptophan were carried out for a total of 3 ns in a simulation box containing 420 water molecules after 1 ns of density equilibration using the NPT protocol with a Berendsen barostat.[48] The Stokes shift correlation function,[55] calculated from tryptophan simulations, was in excellent agreement with both the experimental data[56] and previous computer simulations.[57] This simulation was used as a testing tool for our analysis of the Stokes shift dynamics of PC.

B. Calculations of the Solvation Thermodynamics. Calculations of the solvent reorganization energy and of the solvent part of the reaction free energy ΔG_s were carried out by two methods, (i) nonlocal response function theory (NRFT)[58,59] and (ii) dielectric continuum approximation implemented in the DelPhi program suite.[60] The dielectric constant of TIP3P water ($\epsilon_s = 97.5$[59]) was used for the solvent continuum, and $\epsilon_s = 1$ was used for the protein. This latter choice was driven by our desire to compare continuum and microscopic calculations of the solvation thermodynamics since the latter does not assume any polarization of the protein. In addition, since TIP3P water is nonpolarizable, $\epsilon_\infty = 1.0$ was used for the high-frequency dielectric constant in the reorganization energy calculations. DelPhi[60] numerically solves the Poisson equation of continuum electrostatics to calculate the potential of the dielectric continuum solvent at the positions of charges of the reaction site,

while the NRFT defines the solvent in terms it its nonlocal correlation functions. A full account of the calculations of the redox solvation energy and entropy of PC will be published elsewhere.[61]

In short, the NRFT calculation scheme employs the linear response approximation to replace the solvation chemical potential μ_{0s} with the variance of the solute−solvent interaction potential V_{0s}[58]

$$-\mu_{0s} = (2k_BT)^{-1}\langle(\delta V_{0s})^2\rangle_0 \tag{17}$$

The subscript "0" in the ensemble average $\langle ... \rangle_0$ refers to the fact that, in the linear response approximation, the spectrum of electrostatic fluctuations of the solvent is not perturbed by the electrostatic solute−solvent interactions. Therefore, the variance in eq 17 is calculated for a fictitious system composed of water solvent and the repulsive core of the solute with all solute charges turned off. This approximation is known to work well for dense polar solvents,[59,62] and the main problem of the theory is how to calculate the response function of a polar solvent in the presence of a solute which expels the dipolar polarization field from its volume.[58]

This problem can be solved by applying the Gaussian solvation model,[63] resulting in the linear response function (two-rank tensor) $\chi[\chi_s, \Omega_0]$ functionally depending on the self-correlation function of the dipolar fluctuations of the solvent $\chi_s(\mathbf{k})$ and the shape of the solute occupying volume Ω_0. Once this problem is solved, the solvation chemical potential is calculated as a 3D, inverted-space integral convoluting the electric field of the solute $\tilde{\mathbf{E}}_0(\mathbf{k})$ with the response function

$$-\mu_{0s} = \frac{1}{2}\tilde{\mathbf{E}}_0 * \chi[\chi_s, \Omega_0] * \tilde{\mathbf{E}}_0^* \tag{18}$$

Here, the asterisk refers to both the **k**-integration and tensor contraction, and $\tilde{\mathbf{E}}_0^*$ is the complex conjugate of $\tilde{\mathbf{E}}_0$.

For polar liquids, the function $\chi_s(\mathbf{k})$ splits into projections longitudinal (parallel) and transverse (perpendicular) to the wave vector **k**. Each component is then represented by the corresponding structure factor, which is a function of the magnitude of k only.[58,59] These structure factors were obtained in this work from MD simulations of TIP3P water[49] at different temperatures (see refs 59 and 61 for more details). With this input, the NRFT calculation was performed by grid summation (in **k**-space) of the solvent response function with the solute electric field. This latter was calculated numerically by using fast Fourier transform on the real-space lattice of 512^3 points with a grid spacing of 0.42 Å. In the case of reorganization energy calculations, $\tilde{\mathbf{E}}_0(\mathbf{k})$ in eq 18 is obtained by taking only Δz_j charges of the redox site, thus producing electric field $\Delta\tilde{\mathbf{E}}_0(\mathbf{k})$. In contrast, the solvent component of the free-energy gap of electron transfer, ΔG_s, was calculated with the complete charge distribution of the protein using all $z_k^{(i)}$ atomic charges. In this latter case, one field $\tilde{\mathbf{E}}_0$ in eq 18 is $\Delta\mathbf{E}_0$ and the other is the mean field of the entire protein $\bar{\mathbf{E}}_{prot} = (\tilde{\mathbf{E}}_{prot,1} + \tilde{\mathbf{E}}_{prot,2})/2$.

V. Results

The conformational dynamics of proteins are very disperse,[64] including several time scales that can potentially affect the energetics of electron transfer. Global conformational changes of the protein, which often occur on the time scale of microseconds,[65] give the slowest time scale. These transitions occur between minima of the free-energy landscape separated by the highest barriers. In terms of the two-dimensional coordinate space used in Figure 4, this motion sets up a transition from $q = 0$ to Δq along the generalized protein coordinate q. In Figure 6, we show the cross section of the free-energy surface, $G(X_{02}, q)$, at the final state along the solvent polarization coordinate $X = X_{02}$. The activation barrier separating the states $q = 0$ and Δq is too high to be observed on the time scale of our MD simulations.

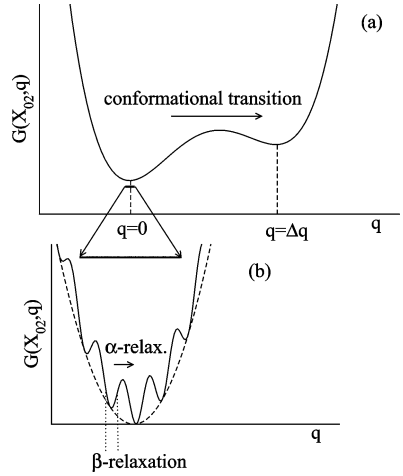

Figure 6. Free-energy landscape for conformational transitions (a) and α-relaxation (b) of the protein. $G(X_{02},q)$ shows the cross section of the two-dimensional free-energy surface taken at the equilibrium final value of the solvent reaction coordinate X_{02}. Each conformational state along the reaction coordinate q contains a large number of substates separated by smaller free-energy barriers (b). Transitions between these states are responsible for α-relaxation of the protein slaved to water dynamics. Each of the α-substates can be separated into β-substates (not shown) responsible for β-relaxation of the protein and the hydration shell.

The topology of the free-energy landscape[66] is, however, more complex than that sketched in Figure 6a. Each of the conformational states, $q = 0$ and Δq, contains a large number of conformational substates separated by lower barriers[19] (Figure 6b). Transitions between these substates represent α-relaxation of the protein with many features analogous to α-relaxation of structural glasses.[67] These protein dynamics are "slaved" to the solvent in a sense that the temperature dependence of the corresponding relaxation time follows that of water.[19] One of the consequences of this slaving is that the long-known dynamical transition of protein atomic displacements above the linear regime at $T_{tr} \simeq 200-250$ K[17,64,67] can be traced back to the fragile-to-strong dynamic transition of hydrating water.[18,68] An alternative explanation suggests a merger of the fast β-relaxation with the slow, nonobservable α-relaxation at the transition temperature.[69]

Fast β-relaxation of the protein and hydrating water can be visualized as transitions between low-barrier substates within each landscape basin of the α-relaxation processes (not shown in Figure 6b). Fluctuations between these substates involve amino acid side chains and a hydrogen-bond network at the protein surface[16,70] as well as protein vibrations which are not affected by the dynamic transition at $T = T_{tr}$. β-relaxation of the protein is strongly dominated by β-relaxation of the hydrating water,[19] involving translational motions of water molecules in and out of the first hydration layer.[16]

This scenario is consistent with the dynamics of the donor−acceptor energy gap observed along the MD simulation trajectory. A large-amplitude, redox-induced conformational transition, if it exists,[71] is too slow to occur on the observation time scale τ_{obs} determined, in the computer experiment, by the length of the simulation trajectory. However, both α- and β-relaxation

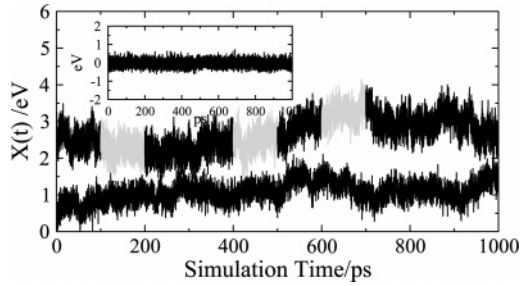

Figure 7. Trajectory of the solvent component of the donor−acceptor energy gap of PC(Ox) in TIP3P water at 310 K. The upper trajectory shows unrestricted protein/water dynamics, and the lower curve refers to protein atomic displacements frozen by applying positional harmonic restrains (8.0 kcal mol^{-1} Å^{-2}). The inset shows the same property for photoexcitation of tryptophan in TIP3P water. The gray regions in the upper trajectory indicate segments of the trajectory 100 ps long used to calculate the narrow free-energy surface in Figure 3a. The lower trajectory was shifted down by 1.5 eV for better visibility.

TABLE 1: Averages and Reorganization Energy Components (eq 9) of the Energy Gap *Y* Based on the Interaction Energy between the Δz_j Charges of the Redox Site with the Solvent (s) and Protein (prot) for PC in Red and Ox States[a]

T/K	redox state	$\langle X\rangle$	$\langle \Delta E_{prot}\rangle$	$\langle Y\rangle$	λ_{prot}	λ_s	λ	$\lambda_{prot,s}$
310	Ox	2.48	−8.58	−6.10	1.62	5.51	6.16	−0.97
	Red	3.39	−8.69	−5.30	1.48	5.66	7.41	0.27
285	Ox	2.46	−8.46	−6.00	1.56	5.09	5.65	−1.00
	Red	3.77	−8.96	−5.19	1.35	4.43	5.25	−0.53

[a] The data are collected from 10 ns MD trajectories; all energies are in eV.

of the protein and water (about 40% of the overall protein relaxation on the 10 ns time scale[37]) are clearly seen in the $X(t)$ trajectory (Figure 7). The slower α-relaxation component is represented by large-amplitude oscillations superimposed onto fast β-fluctuations of the solvent dipoles. The slow α-relaxation is not typically seen in small rigid solutes exemplified by the trajectory of tryptophan (inset in Figure 7) where only fast β-fluctuations are present. The time scale of α-fluctuations (ca. 1 ns) suggests their origin in the motion of polar side groups,[69] which show jumps in their dihedral angles on the same time scale.[72]

A. Interactions with Water and Protein. Table 1 lists the statistics of *Y* fluctuations obtained at 10 ns from the end of the simulation trajectories. We report the average donor−acceptor energy gap from the interaction of Δz_j charges (Table S1) of the redox site (Red and Ox states) with water, $\langle X\rangle$, and protein, $\langle \Delta E_{prot}\rangle$, as well as their sum, $\langle Y\rangle$ (we have dropped Ox/Red subscripts in the ensemble averages for brevity). In addition, Table 1 gives the variance of *Y* which is split, according to eq 9, into protein and water (solvent) components. The cross term $\lambda_{prot,s}$ amounts in our simulations to 5−18% of the total reorganization energy from the protein/water thermal bath. This is the error bar for the separation of protein and solvent (water) nuclear fluctuations into two separate stochastic processes.

B. Solvent Reorganization Energy. The reorganization energy $\lambda_q(\tau_{obs})$ in eq 10 originates from fluctuations of the solvent dipolar polarization induced by coupled protein/solvent dynamics. This reorganization energy thus arises from a new solvent mode absent in traditional theories of electron transfer operating in terms of separate vibrational (λ_v) and polarization (λ_p) nuclear modes. The enhancement of the energy gap variance by this new mode is very significant; the variance of *X* changes from $\sigma_s^2 = 2k_BT\lambda_p$ ($\lambda_p = \Delta X/2 \simeq 0.45-0.65$eV), comparable to other simulations,[8,26] to a much higher value $\sigma_s^2 = 2k_BT\lambda_s$ characterized by the solvent reorganization energy $\lambda_s = \lambda_p + \lambda_q(\tau_{obs}) \simeq 5$ eV on the time scale $\tau_{obs} \simeq 10$ ns (Table 2). This gigantic value of the reorganization energy far exceeds what is typically observed for electron-transfer reactions between small hydrated ions.[25,73,74]

TABLE 2: Solvent Reorganization Parameters of PC from 10 ns MD Trajectories (All Energies Are in eV)

T/K	λ_p	λ_q	ΔG_s[a]
285	0.81[b]	4.8(Red)	3.2
	0.77 (0.69,3.6)[c]	4.1(Ox)	4.7 (7.1, 9.6)[c]
310	0.54[b]	5.0(Red)	2.9
	0.74 (0.54,3.6)[c]	4.5(Ox)	4.6 (7.1, 9.6)[c]

[a] Solvent component of the redox free energy obtained from the simulation data as $\Delta G_s = G_s^{Ox} - G_s^{Red} = (X_{01} + X_{02})/2$. [b] Calculated from the simulation data as $(X_{01} - X_{02})/2$ (eq 4). [c] Theoretical calculations using atomic charges, vdW radii, and coordinates of the protein combined with microscopic, nonlocal response functions of water.[58,59] Dielectric continuum calculations using DelPhi[60] (parentheses) have been done with the solvent-accessible cavity (first number) and the standard vdW cavity (second number).[61]

The variance of the donor−acceptor energy gap $\sigma_q \simeq 0.5$ eV (eq 16) produced by conformational flexibility in our simulations is significantly higher than experimentally reported $\sigma_q \simeq 0.05$ eV from charge recombination in bacterial reaction centers trapped by cooling in their conformational substates.[37] As noted above, this lower variance of energy gaps in reaction centers is expected since water dynamics, significantly contributing to fluctuations of the donor−acceptor energy gap, are also quenched by cooling. In addition, the hydrophobic environment of cofactors located in the membrane protein complex and the low temperature of the kinetic arrest $T_{kin} \simeq 175$ K (eq 16) both contribute to a lower σ_q.

We need to emphasize that the reorganization energies considered here refer to the change in the charge distribution of PC only. A donor−acceptor complex composed of two proteins (interprotein electron transfer) will also include a change of charges on the partner (heme) protein. In the case of photosynthetic electron transfer, the interaction of this other set of charges located within a membrane protein with water is expected to be weaker than that for hydrated PC. Therefore, there should be only minor Coulomb correction to the reorganization energy. In addition, some reduction of the reorganization energy will arise from the electronic polarizability of water not included in the TIP3P parametrization (our calculations using nonlocal solvent response[58,59] show a reduction from 0.74 eV in TIP3P water to 0.40 eV in ambient water). Nevertheless, the gigantic magnitude of $\lambda_p + \lambda_q(10\text{ ns})$ compared to the commonly considered λ_p calls for the attention to the effects of coupled protein/water dynamics on electron transfer.

The solvent effect on the electron-transfer thermodynamics is dominated by water molecules closest to the active site. Protein flexibility significantly modulates this first solvation shell, producing fluctuations of the closest Cu−O distance around the average of 6.64 Å, the largest fluctuation amplitude of ≃2 Å, and the standard deviation of 0.6 Å (Figure 8). We also note that the Cu−O pair distribution function (Figure S1) does not change with changing of the redox state of plastocyanin, in contrast to observations reported for heme proteins.[8,11,12,26] With such large-amplitude fluctuations, water is effectively further apart from the protein surface than the distance of the closest approach. The solvent part of the reaction free energy ΔG_s (Table 2) is then nearly 1.5 times smaller in magnitude than the value calculated from our solvation model[58,59]

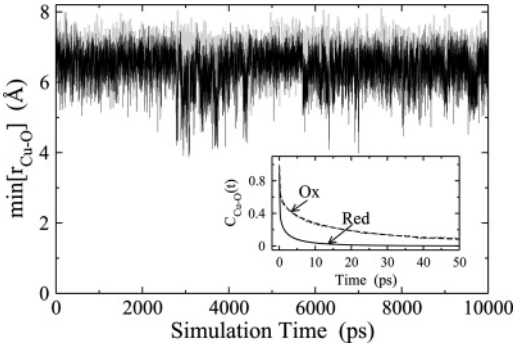

Figure 8. Trajectory of the closest distance between Cu of the plastocyanin-active site (Figure 1) and the oxygen of water in the Red (gray) and Ox (black) states. The inset shows time autocorrelation functions of the minimum Cu−O distance in Red and Ox states. The autocorrelation functions fit well to eq 20 with the set of fitting parameters $\{A_G,\tau_G,\tau_E,\beta\}$ of {0.31,0.2,12.3,0.53} for Ox and {0.39, 0.2,1.1,0.46} for Red. Here, τ_G and τ_E are in picoseconds.

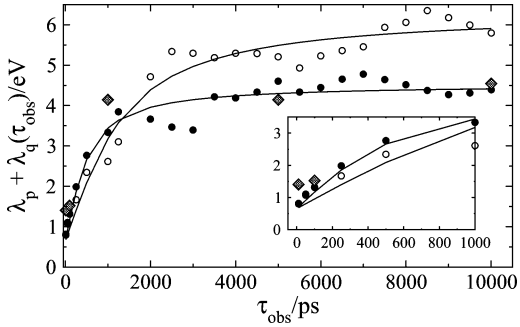

Figure 9. Solvent (water) reorganization energy of Ox (open circles) and Red (filled circles) states of PC at 285 K versus the observation time τ_{obs} defined as the length of the trajectory over which the averages were calculated. The solid lines are fits of simulations to eq 19 with τ_q = 1 ns (Ox) and τ_q = 0.5 ns (Red). The hatched diamonds indicate the results from ref 11. The inset shows the initial portion of the plot.

assuming the closest water approach. In contrast, the calculated reorganization energy λ_p is in good agreement with simulations, which supports our assumption used to derive eqs 10 and 11 that conformational fluctuations do not significantly affect this parameter.

We note in passing that λ_p from continuum calculations is very sensitive to the definition of the dielectric cavity. When van der Waals (vdW) radii of protein atoms are used to determine the cavity, the high-polarity dielectric is allowed in a narrow pocket near copper, thus significantly increasing the free energy of solvation. When, in contrast, a water molecule is rolled on the vdW surface to determine the solvent-accessible cavity, the results of continuum calculations are comparable to both the NRFT and MD numbers (Table 2). We will provide a more detailed discussion of these results in a separate publication.[61]

The large value of λ_q raises the question of whether the new nuclear mode responsible for the energy gap variation should be attributed solely to the conformational motions of the protein or to more complex collective dynamics coupling the solvent to protein fluctuations. The evidence existing in the literature advocates the latter view, suggesting that both the α- and β-relaxation of the protein are strongly coupled to hydrating water. Our attempts to connect the slow modulations of the $X(t)$ trajectory (Figure 7) to the vibrational density of states of the protein[75] have not given positive results since the low-frequency vibrations seen in Figure 7 could not be resolved from the quasi-harmonic analysis[75] (Figure S2) or from the intermediate scattering function.[17] We have also tried to freeze the protein motions through harmonic positional restraints on atomic translations, with the restraint weight equal to 8.0 kcal mol^{-1} Å^{-2}. These simulations (ca. 5 ns started at the end of the unrestrained trajectory) have resulted in the energy gap variance σ_s^2 diminished by a factor of ≃3 (lower trajectory in Figure 7) but still not reaching the value σ_p^2 from the Stokes shift. This observation supports the view that α-fluctuations of the donor−acceptor gap are coupled to translational motions within the hydration layer at the protein surface and that these fluctuations cannot be separated from the protein's conformational dynamics. Nevertheless, the strong reduction of σ_s^2 upon freezing of the protein still suggests that protein motions produce the largest energetic contribution to the reorganization energy λ_q.

C. Protein Dynamics. If the large-amplitude protein/water motions affecting the solvent polarization are overdamped,[76] they can be described by Debye relaxation with an effective relaxation time τ_q. The use of the Debye relaxation function in eq 14 gives the following simple equation for the non-ergodic reorganization energy[77]

$$\lambda_q(\tau_{obs}) = (2\lambda_q/\pi)\cot^{-1}(\tau_q/\tau_{obs}) \tag{19}$$

where the equilibrium reorganization energy λ_q is given by eq 15. Protein dynamics coupled to dipolar solvent polarization are dominated by very slow motions, with the characteristic time τ_q of about 0.5−1 ns, as follows from the fit of $\lambda_p + \lambda_q(\tau_{obs})$ (eq 19) to the simulation data (Figure 9). The non-ergodic component $\lambda_q(\tau_{obs})$ was calculated from the energy gap variance taken on observation windows τ_{obs} along the simulation trajectory (exemplified by gray segments of length 100 ps in Figure 7). On short observation times, τ_{obs} < 100 ps, that is, fast electron-transfer reactions, the slow conformational modulation does not show up, and the reorganization energy from the width approaches that from the Stokes shift, thus restoring eq 3. A similar behavior, including the magnitude of the corresponding reorganization energy, was observed in ref 11 (hatched diamonds in Figure 9).

With such slow conformational modulation of the water polarization, each short segment of the long trajectory finds itself in a different configuration, a situation akin to dynamical heterogeneity responsible for stretched-exponential relaxation of structural glasses.[67] This picture is indeed confirmed by the Stokes shift correlation function calculated on segments of the trajectory of different lengths. The Stokes shift correlation function $C(t) = \langle X(t)X(0)\rangle$ from a short segment has a typical biphasic form composed of a fast Gaussian decay followed by exponential relaxation,[55] for which the stretching exponent β in eq 20 is equal to unity

$$C(t) = A_G e^{-(t/\tau_G)^2} + (1 - A_G)e^{-(t/\tau_E)^\beta} \tag{20}$$

On the contrary, the Stokes shift correlation function calculated on longer segments (1−2 ns) develops a stretched-exponential relaxation with the stretching exponent of β = 0.69 and relaxation time of about 150 ps (Figure S3). This long tail, which may require longer simulations to be fully resolved,[37] is caused by collective water displacements (Figures 1 and 5) by slowly moving parts of a biopolymer.[57,78]

D. Free-Energy Surfaces. The picture of non-ergodic, glassy dynamics emerging from the static and time-resolved energy gap statistics is consistent with the free-energy surfaces $G_i(X)$ shown in Figure 3. They are very shallow on the long 10 ns trajectory, becoming increasingly curved on a shorter observa-

tion window (Figure 3a). The slow non-ergodic dynamics of protein conformations decouples the Stokes shift from the reorganization energy, thus breaking eq 3 down. Accordingly, we found that the difference $G_2(X) - G_1(X)$ in the region of overlap of Ox and Red surfaces is still a linear function of X but with the slope of 0.10 instead of the unitary slope predicted by the picture of equal-curvature parabolas (eq 2 and Figure 2) and usually observed in fully equilibrated systems.[11] This number is consistent with eqs 10 and 11, which yield the slope of $\Delta X/(\Delta X + 2\lambda_q) \simeq 0.13$.

The statistics of the donor−acceptor energy gap induced by the protein fluctuations are also approximately Gaussian. The width of the distribution is given by the variance of the electrostatic interaction energy of Δz_j charges of the redox site with the protein atomic charges. The corresponding reorganization energy is approximately 1.5 eV (Table 2). However, since the reaction path is expected to follow the fast solvent coordinate, our main focus here is on the free energies $G_i(X)$.

These results do not contradict experimental estimates of $\lambda_p + \lambda_v \simeq 0.6-0.8$ eV for copper proteins obtained from the top of the energy gap law when the reaction barrier disappears.[5,13] From eq 11, the activationless transition is achieved at $X_{0i} = 0$ when the reaction free energy ΔG_0 obeys the equation $-\Delta G_0 - \lambda_v = \Delta X/2 = \lambda_p$. With the inner vibrational reorganization energy currently estimated as low as 0.1 eV,[8] $\lambda_p = 0.54-0.81$ eV from present simulations is consistent with experiment. On the other hand, reorganization energy λ_s entering the distribution width σ_s^2 is about an order of magnitude higher. The breakdown of the link between the Stokes shift and the distribution width (eq 3) must have significant implications on the biological function of PC and probably of other electron carrier proteins. We note that a similarly large value of λ_q (hatched diamonds in Figure 9) was observed, but not clearly recognized, in simulations of electron transfer between ruthenium cofactors attached to a synthetic four-helix protein.[11]

VI. Concluding Remarks

The application of the ideas presented here to biological electron transfer requires the transition from the observation time determined by the length of the simulation trajectory to the time scale determined by reaction kinetics. This is achieved by setting $\tau_{obs} = \tau_{ET} = k_{ET}^{-1}$, which, given that the activation barrier is a function of τ_{obs}, leads to a self-consistent equation for the rate[31]

$$k_{ET} \propto \exp[-\Delta G^{act}(k_{ET})/(k_B T)] \qquad (21)$$

Equation 21, incorporating the notion of reaction non-ergodicity, offers a compelling picture of the hierarchy of electron-transfer reactions in photosynthetic systems. Faster reactions with $k_{ET} \gg 10^9$ s^{-1} effectively cut off slow conformational motions of the protein from their energetics (Figure 9), and the standard picture[6] relating the Stokes shift to the parabolas' curvatures (eq 3) applies. Realizing fast electron transfer then requires an activationless transition, as observed in primary charge separation in photosynthetic reaction centers (Figure 10a).[20] On the contrary, reactions in the subnanosecond range start to experience the effect of conformational modulation of the activation barrier and can, in fact, proceed efficiently even with a small driving force since the activation barrier is lowered by the growing width of the energy gap distribution (Figure 10b). Therefore, when speed is at stake, natural systems have to lose redox potential in exchange for fast activationless transitions. When slower reactions, still faster than catalytic rates, can be afforded, losing the reduction potential is not a necessity, and reactions with a low driving force can still be efficient.

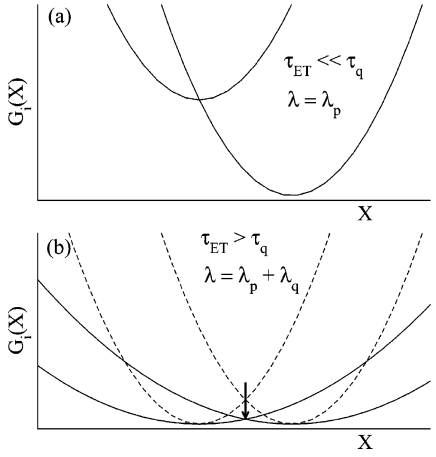

Figure 10. Energetics of fast electron-transfer reactions losing redox potential to achieve activationless transitions (a) and of slower (ns range) reactions (b) which are allowed to proceed with a small driving force. The reaction barrier is lowered in the latter case by non-ergodic conformational/water dynamics transforming the dashed-line parabolas into solid-line parabolas (b). The vertical arrow in (b) shows the suppression of the activation barrier by the reorganization energy λ_q.

The large breadth of energy gap fluctuations observed here allows relaxation of the strict limitations on the closest distance of docking in interprotein electron transfer. The activation barrier estimated from our simulated reorganization energies is extremely small, $\Delta G^{act} = (\lambda_p + \Delta G_0)^2/(4\lambda_p + 4\lambda_q) \simeq 0.08$eV, for a small reaction free energy of $\Delta G_0 \simeq -20$ meV typical for electron transfer at docking locations.[4] The standard rate estimate[3] then gives 13 Å for the donor−acceptor distance at which the threshold catalytic rate of 10^4 s^{-1} is achieved.

Strong coupling between dipolar polarization and protein mobility advocated here is consistent with the long-suggested connection between protein dynamics and hydration.[16,18,19,68,69] The new reorganization energy discovered here is related to the rms displacement of the conformational mode as $\lambda_q \propto \langle(\delta q)^2\rangle/T$ and is therefore expected to show a sharp increase at $T > T_{tr}$ when $\langle(\delta q)^2\rangle$ starts its nonlinear rise. This observation might provide a resolution of the long-standing puzzle of electron-transfer kinetics in many plants and bacteria: Arrhenius plots of electron-transfer rates often show breaks in their slopes at temperatures consistent with T_{tr}.[79−81] This feature might be linked to the rise of λ_q at the onset of conformational activity in proteins.[82]

The existence of the solvent-slaved α-relaxation is presently traced back to a strong coupling between polar/ionized surface residues and water. We suggest in this paper that exactly this property is responsible for the strong modulation of the dipolar polarization of water by protein flexibility, resulting in the gigantic solvent reorganization energy. This type of dynamics is usually not observed in inorganic and organic donor−acceptor complexes used for electron-transfer reactions and is presently believed to be unique to natural polymers. However, properties of synthetic polymers, in particular, in respect to glassy dynamics,[83] have many features in common with biopolymers. One therefore might hope that phenomena analogous to those observed here can be realized in flexible donor−acceptor architectures, such as branched polymers and dendrimeric structures, used for artificial photosynthesis.

Acknowledgment. This work was supported by the NSF (CHE-0616646). CPU time was provided by Pittsburgh Super-

computer Center and ASU's Center for High Performance Computing. We are grateful to Marshall Newton for critical comments on the manuscript.

Supporting Information Available: Atomic charges of the redox site and Figures S1−S3. This material is available free of charge via the Internet at http://pubs.acs.org.

References and Notes

(1) Gray, H. B.; Winkler, J. R. *Proc. Natl. Acad. Sci., U.S.A.* **2005**, *102*, 3534.
(2) Warshel, A.; Parson, W. W. *Quat. Rev. Biophys.* **2001**, *34*, 563.
(3) Noy, D.; Moser, C. C.; Dutton, P. L. *Biochim. Biophys. Acta* **2006**, *1757*, 90.
(4) Ubbink, M.; Ejdebäck, M.; Karlsson, B. G.; Bendall, D. S. *Structure* **1998**, *6*, 323.
(5) Gray, H. B.; Malmström, B. G.; Williams, R. *J. Biol. Inorg. Chem.* **2000**, *5*, 551.
(6) Marcus, R. A.; Sutin, N. *Biochim. Biophys. Acta* **1985**, *811*, 265.
(7) Solomon, E.; Szilagyi, R.; DeBeerGeorge, S.; Basumallick, L. *Chem. Rev.* **2004**, *104*, 419.
(8) Cascella, M.; Magistrato, A.; Tavernelli, I.; Carloni, P.; Rothlisberger, U. *Proc. Natl. Acad. Sci. U.S.A.* **2006**, *103*, 19641.
(9) Muegge, I.; Qi, P. X.; Wand, A. J.; Chu, Z. T.; Warshel, A. *J. Phys. Chem. B* **1997**, *101*, 825.
(10) Olsson, M.; Hong, G.; Warshel, A. *J. Am. Chem. Soc.* **2003**, *125*, 5025.
(11) Blumberger, J.; Klein, M. L. *J. Am. Chem. Soc.* **2006**, *128*, 13854.
(12) Sulpizi, M.; Raugei, S.; VandeVondele, J.; Carloni, P.; Sprik, M. *J. Phys. Chem. B* **2007**, *111*, 3969.
(13) Skov, L.; Pascher, T.; Winkler, J.; Gray, H. *J. Am. Chem. Soc.* **1998**, *120*, 1102.
(14) Hoffman, B. M.; Celis, L. M.; Cull, D. A.; Patel, A. D.; Seifert, J. L.; Wheeler, K. E.; Wang, J.; Yao, J.; Kurnikov, I. V.; Nocek, J. M. *Proc. Natl. Acad. Sci. U.S.A.* **2005**, *102*, 3564.
(15) Skourtis, S. S.; Balabin, I. A.; Kawatsu, T.; Beratan, D. N. *Proc. Natl. Acad. Sci. U.S.A.* **2005**, *102*, 3552.
(16) Tarek, M.; Tobias, D. J. *Phys. Rev. Lett.* **2002**, *88*, 138101.
(17) Bizzarri, A. R. *J. Phys.: Condens. Matter* **2004**, *16*, R83.
(18) Chen, S.-H.; Liu, L.; Fratini, E.; Baglioni, P.; Faraone, A.; Mamontov, E. *Proc. Natl. Acad. Sci. U.S.A.* **2006**, *103*, 9012.
(19) Fenimore, P. W.; Frauenfelder, H.; McMahon, B. H.; Young, R. D. *Proc. Natl. Acad. Sci. U.S.A.* **2004**, *101*, 14408.
(20) Bixon, M.; Jortner, J. *Adv. Chem. Phys.* **1999**, *106*, 35.
(21) Lax, M. *J. Chem. Phys.* **1952**, *20*, 1752.
(22) Hwang, J.-K.; Warshel, A. *J. Am. Chem. Soc.* **1987**, *109*, 715.
(23) Matyushov, D. V.; Schmid, R. *J. Chem. Phys.* **1995**, *103*, 2034.
(24) Sterpone, F.; Ceccarelli, M.; Marchi, M. *J. Phys. Chem. B* **2003**, *107*, 11208.
(25) Kuharski, R. A.; Bader, J. S.; Chandler, D.; Sprik, M.; Klein, M. L.; Impey, R. W. *J. Chem. Phys.* **1988**, *89*, 3248.
(26) Simonson, T. *Proc. Natl. Acad. Sci. U.S.A.* **2002**, *99*, 6544.
(27) Marcus, R. A. *J. Phys. Chem.* **1989**, *93*, 3078.
(28) Ungar, L. W.; Newton, M. D.; Voth, G. A. *J. Phys. Chem. B* **1999**, *103*, 7367.
(29) Hartnig, C.; Koper, M. T. M. *J. Chem. Phys.* **2001**, *115*, 8540.
(30) Blumberger, J.; Sprik, M. *J. Phys. Chem. B* **2005**, *109*, 6793.
(31) Matyushov, D. V. *Acc. Chem. Res.* **2007**, *40*, 294.
(32) Matyushov, D. V. *Chem. Phys. Lett.* **1993**, *203*, 131.
(33) Hatcher, E.; Soudackov, A.; Hammes-Schiffer, S. *Chem. Phys.* **2005**, *319*, 93.
(34) Mukamel, S. *Principles of Nonlinear Optical Spectroscopy;* Oxford University Press: New York, 1995.
(35) Frauenfelder, H.; Sligar, S. G.; Wolynes, P. G. *Science* **1991**, *254*, 1598.
(36) Gehlen, J. N.; Marchi, M.; Chandler, D. *Science* **1994**, *263*, 499.
(37) McMahon, B. H.; Müller, J. D.; Wraight, C. A.; Nienhaus, G. U. *Biophys. J.* **1998**, *74*, 2567.
(38) Lieble, U.; Lipowski, G.; Négrerie, M.; Lambry, J.-C.; Martin, J.-L.; Vos, M. H. *Nature* **1999**, *401*, 181.
(39) Min, W.; Luo, G.; Cherayil, B. J.; Kou, S. C.; Xie, X. S. *Phys. Rev. Lett.* **2005**, *94*, 198302.
(40) Agmon, N.; Hopfield, J. J. *J. Chem. Phys.* **1983**, *78*, 6947.
(41) Sumi, H.; Marcus, R. A. *J. Chem. Phys.* **1986**, *84*, 4894.
(42) Walker, G. C.; Aakesson, E.; Johnson, A. E.; Levinger, N. E.; Barbara, P. F. *J. Phys. Chem.* **1992**, *96*, 3728.
(43) Hoffman, B. M.; Ratner, M. A. *Inorg. Chim. Acta* **1996**, *243*, 233.
(44) Medvedev, E. S.; Kotelnikov, A. I.; Goryachev, N. S.; Psikha, B. L.; Ortega, J. M.; Stuchebrukhov, A. A. *Mol. Simul.* **2006**, *32*, 735.
(45) Hodge, I. M. *J. Non-Cryst. Solids* **1994**, *169*, 211.
(46) Case, D. A.; Cheathamm T. E., III; Darden, T.; Gohlke, H.; Luo, R.; Merz, K. M., Jr.; Onufriev, A.; Simmerling, C.; Wang, B.; Woods, R. J. *J. Comput. Chem.* **2005**, *26*, 1668.
(47) Xue, Y.; Okvist, M.; Hansson, O.; Young, S. *Protein Sci.* **1998**, *7*, 2099.
(48) Berendsen, H. J. C.; Postma, J. P. M.; van Gunsteren, W. F.; DiNola, A.; Haak, J. R. *J. Chem. Phys.* **1984**, *81*, 3684.
(49) Jorgensen, W. L.; Chandrasekhar, J.; Madura, J. D.; Impey, R. W.; Klein, M. L. *J. Chem. Phys.* **1983**, *79*, 926.
(50) Duan, Y.; Wu, C.; Chowdhury, S.; Lee, M. C.; Xiong, G.; Zhang, W.; Yang, R.; Cieplak, P.; Luo, R.; Lee, T.; Caldwell, J.; Wang, J.; Kollman, P. *J. Comput. Chem.* **2003**, *24*, 1999.
(51) Ullmann, G. M.; Knapp, E.-W.; Kostić, N. M. *J. Am. Chem. Soc.* **1997**, *119*, 42.
(52) Kerpel, J. O. D.; Ryde, U. *Proteins: Struct., Funct., Genet.* **1999**, *36*, 157.
(53) Hassanali, A.; Li, T.; Zhong, D.; Singer, S. *J. Phys. Chem. B* **2006**, *110*, 10497.
(54) Sobolewski, A. L.; Domcke, W. *Chem. Phys. Lett.* **1999**, *315*, 293.
(55) Jimenez, R.; Fleming, G. R.; Kumar, P. V.; Maroncelli, M. *Nature* **1994**, *369*, 471.
(56) Pal, S. K.; Zewail, A. H. *Chem. Rev.* **2004**, *104*, 2099.
(57) Nilsson, L.; Halle, B. *Proc. Natl. Acad. Sci. U.S.A.* **2005**, *102*, 13867.
(58) Matyushov, D. V. *J. Chem. Phys.* **2004**, *120*, 7532.
(59) Milischuk, A. A.; Matyushov, D. V.; Newton, M. D. *Chem. Phys.* **2006**, *324*, 172.
(60) Rocchia, W.; Sridharan, S.; Nicholls, A.; Alexov, E.; Chiabrera, A.; Honig, B. *J. Comput. Chem.* **2002**, *23*, 128.
(61) LeBard, D. N.; Matyushov, D. V. *J. Chem. Phys.* **2008**, submitted.
(62) LeBard, D. N.; Lilichenko, M.; Matyushov, D. V.; Berlin, Y. A.; Ratner, M. A. *J. Phys. Chem. B* **2003**, *107*, 14509.
(63) Chandler, D. *Phys. Rev. E* **1993**, *48*, 2898.
(64) Frauenfelder, H.; Parak, F.; Young, R. D. *Annu. Rev. Biophys. Biophys. Chem.* **1998**, *17*, 451.
(65) Fenimore, P. W.; Frauenfelder, H.; McMahon, B. H.; Parak, F. G. *Proc. Natl. Acad. Sci. U.S.A.* **2002**, *99*, 16047.
(66) Stillinger, F. H. *Science* **1995**, *267*, 1935.
(67) Angell, C. A. *Science* **1995**, *267*, 1924.
(68) Caliskan, G.; Briber, R. M.; Thirumalai, D.; Garcia-Sakai, V.; Woodson, S. A.; Sokolov, A. P. *J. Am. Chem. Soc.* **2005**, *128*, 32.
(69) Swenson, J.; Jansson, H.; Hedsröm, J.; Bergman, R. *J. Phys.: Condens. Matter* **2007**, *19*, 205109.
(70) Engler, N.; Ostermann, A.; Niimura, N.; Parak, F. G. *Proc. Natl. Acad. Sci. U.S.A.* **2003**, *100*, 10243.
(71) A redox-induced change in the secondary structure was suggested based on infrared spectroscopy. This observation, however, contradicts to the available X-ray data; see discussion in Taneva, S. G.; Kaiser, U.; Donchev, A. A.; Dimitrov, M. I.; Mäntele, W.; Muga, A. *Biochemistry* **1999**, *38*, 9640.
(72) Baysal, C.; Atilgan, A. R. *Biophys. J.* **2005**, *88*, 1570.
(73) Elliott, C. M.; Derr, D. L.; Matyushov, D. V.; Newton, M. D. *J. Am. Chem. Soc.* **1998**, *120*, 11714.
(74) Newton, M. D. *Adv. Chem. Phys.* **1999**, *106*, 303.
(75) Go, N.; Noguti, T.; Nishikawa, T. *Proc. Natl. Acad. Sci. U.S.A.* **1983**, *80*, 3696.
(76) Markelz, A. G.; Knab, J. R.; Chen, J. Y.; He, Y. *Chem. Phys. Lett.* **2007**, *442*, 413.
(77) Ghorai, P. K.; Matyushov, D. V. *J. Chem. Phys.* **2006**, *124*, 144510.
(78) Andreatta, D.; Pérez, J. L.; Kovalenko, S. A.; Ernsting, N. P.; Murphy, C. J.; Coleman, R. S.; Berg, M. A. *J. Am. Chem. Soc.* **2005**, *127*, 7270.
(79) de Vault, D.; Chance, B. *Biophys. J.* **1966**, *6*, 825.
(80) Hales, B. J. *Biophys. J.* **1976**, *16*, 471.
(81) Borovikh, I. V.; Gast, P.; Dzuba, S. A. *J. Phys. Chem. B* **2005**, *109*, 7535.
(82) Parak, F. G. *Rep. Prog. Phys.* **2003**, *66*, 103.
(83) Frick, B.; Richter, D. *Science* **1995**, *267*, 1939.